Available online at www.sciencedirect.com
SCIENCE DIRECT
Journal of Catalysis 228 (2004) 311–320
JOURNAL OF CATALYSIS
www.elsevier.com/locate/jcat

$CuCl_2$ immobilized on amino-functionalized MCM-41 and MCM-48 and their catalytic performance toward the vapor-phase oxy-carbonylation of methanol to dimethylcarbonate

Youzhu Yuan *, Wei Cao, Weizheng Weng

State Key Laboratory of Physical Chemistry of Solid Surfaces, Department of Chemistry, Xiamen University, Xiamen 361005, China

Received 2 June 2004; revised 30 August 2004; accepted 3 September 2004

Available online 22 October 2004

Abstract

Amino-functionalized MCM-41 and MCM-48 mesoporous silicas were used to immobilize $CuCl_2$ for the vapor-phase oxy-carbonylation of methanol to produce DMC. Higher reaction rates and better catalytic stability were obtained with $CuCl_2$ supported onto amino-functionalized MCM-41 and MCM-48 in the DMC yield in comparison with those with $CuCl_2$ supported on nonfunctionalized mesoporous silicas under identical conditions. The best DMC yield was obtained with a $CuCl_2$ loading of about 10 wt%, which corresponds to the N/Cu atomic ratios of 1.5 and 2.4 in the $CuCl_2$/1N-MCM-41 and $CuCl_2$/2N-MCM-41, respectively. Characterizations with XRD, N_2 adsorption, XPS, and HRTEM revealed that the regular hexagonal/cubic arrays in MCM-41 and MCM-48 were retained after the amino-functionalization and the immobilization of $CuCl_2$ with a loading weight lower than 20 wt%. The Cu species in the catalysts with loadings lower than 10 wt% were mainly located and finely dispersed in the mesopores of amino-functionalized MCM-41 and MCM-48 through a coordinative complexation with the amino groups, forming $(N)_2 \rightarrow Cu^{2+}$ complex species. The better performance of $CuCl_2$ on amino-functionalized MCM-41 and MCM-48 for the DMC production via vapor-phase oxy-carbonylation of methanol may be ascribed to the high dispersion of active sites at regular mesopores, in addition to the accelerated redox process of Cu^{2+}/Cu^{+} in the complex species.

Keywords: MCM-41; MCM-48; Amino-functionalization; Copper catalyst; Methanol; Oxy-carbonylation; Dimethylcarbonate

1. Introduction

Mesoporous molecular sieves synthesized with the aid of micelle templates have shown huge surface areas, well-ordered periodic structures, and controllable pore sizes by varying the template molecule and/or using additives such as trimethylbenzene [1]. These characteristics of mesoporous molecular sieves make them attractive in the search for novel catalysts for chemical reactions. Representatively, the modification of mesoporous materials by grafting metal complexes is an important area of research in heterogeneous catalysis [2]. One of the best pathways has already been achieved by anchorage of neutral ligand onto silica through covalent Si–O–Si bonds [3–8]. The neutral ligands were mainly amine or phosphine functions directly grafted to the silica surface by a silylation procedure. These types of ligands permitted immobilization of metal complexes, through a coordination bond with metal centers. Brunel and co-workers have used 3-aminopropyltrimethoxysilane and 3-chloropropyltriethoxysilane as intermediates for grafting amino functionality and functionalized alkoxysilanes to MCM-41 [9–11]. By a similar methodology, manganese(III) Schiff base complexes were added to modified MCM-41 [11]. The immobilization of cobalt chelate complexes onto MCM-41 was performed through methoxysilyl coupling agents functionalized with ethylenediamine, diethylenetriamine, and ethylenetriacetic acid salt. The resulting materials showed some reactivity toward forming oxygen adducts [12]. FSM-type mesoporous silicas with differ-

* Corresponding author. Fax: +86-592-2183047.
E-mail address: yzyuan@xmu.edu.cn (Y. Yuan).

0021-9517/$ – see front matter
doi:10.1016/j.jcat.2004.09.003

ent densities of silanol groups have been silylated using chloroalkyldimethylsilane and aminopropyltrimethoxysilanes [13]. In addition, the hexagonal mesoporous silica (HMS), which was produced by a low concentration of the neutral template according to the route of S^0I^0, has been grafted with amines by using dimethylaminopropyl groups. The prepared materials showed high activities toward the Michael addition [14]. Evans and co-workers showed that the grafted amino ligand covalently bonded to the internal pore surface of highly ordered HMS through a silylation procedure and the immobilized transition-metal–aquo complexes such as Mn^{II}–aquo, Cu^{II}–aquo, Co^{II}–aquo, and Zn^{II}–aquo were coordinated to the supported wall without impregnation on the surface. The resulting silica materials have opened new opportunities in various applicable fields, particularly in the study of the kinetics of redox reactions [15].

It is known that the formation of dimethylcarbonate (DMC) molecules from oxy-carbonylation of MeOH with CO requires an oxidation process involving transfer of two electrons. Many catalyst systems containing $CuCl_2$/CuCl have been screened for the selective methanol oxy-carbonylation to DMC with one-step liquid-phase or gas-phase processes [16–27]. Romano and co-workers at EniChem Company have developed a one-step slurry process running continuously at industrial scale to make DMC from methanol, carbon monoxide, and oxygen following the oxy-carbonylation by employing cuprous chloride as a catalyst which was suspended in a methanol liquid phase during the reaction [16,17]. They suggested that the reaction involved two steps: oxidation and reduction [17]. Curuntt et al. had tested a number of catalysts for the one-step gas-phase oxy-carbonylation of methanol to DMC [18]. The catalysts were prepared by impregnating the active carbon or oxide (MnO, ZnO, TiO_2, SiO_2, and Al_2O_3) in a methanol solution of $[Cu(OCH_3)(pyridine)Cl]_2$ or/and $CuCl_2$. All of the tested catalysts deactivated quickly because of the loss of chlorine and the formation of paratacamite $[Cu_2(OH)_3Cl]_2$ on the supports. King [19,20] reported that Cu^IY catalysts (almost free of chlorine) made by the high-temperature solid-state ion exchange of CuCl with HY zeolite under flowing helium had higher and more stable activity than those made by solution ion exchange of $CuCl_2$ with the HY zeolite or impregnation of $CuCl_2$ on the active carbon. Slade and co-workers [21] showed that the use of MCM-41 to support CuCl through solid-state ion exchange under flowing N_2 could afford a catalyst with higher selectivity of methanol to DMC.

The factors that could accelerate the redox cycle of the active centers like Cu^{2+}/Cu^+ would be beneficial for the reaction rate. Considerable enhancements in the methanol conversion and selectivity to DMC have been observed by using supported and unsupported copper-based catalysts modified with N-/P-donor ligands [28–32]. Representatively, a kind of nitrogen-containing polymer-supported $CuCl_2$ has been developed by Souma and co-workers as good catalysts for the liquid reaction of DMC synthesis [28–30]. It was reported that the CuCl immobilized on diamide-modified SBA-15 was an efficient heterogenized catalyst for the oxy-carbonylation of methanol to DMC [32]. Quite recently, we have reported an efficient heterogeneous catalyst system for the vapor-phase oxy-carbonylation of methanol to produce DMC by supporting $CuCl_2$ on amino-functionalized mesoporous silicas MCM-41 and MCM-48 [33].

The present study reports, in detail, the performance of supported Cu catalysts for the selective oxy-carbonylation of methanol to produce DMC, the effects of the support and the Cu-loading on the performance, and the characterization of the active Cu species by means of XRD, BET, XPS, TG-DTA, HRTEM, and FTIR.

2. Experimental

2.1. Catalyst preparation

The mesoporous silicas of MCM-41 and MCM-48 were obtained according to the literature procedures [34]. Amino-functionalized mesoporous silicas were prepared respectively with 3-aminopropyltrimethoxysilane (Aldrich) or *N*-[(3-trimethoxysilyl)propyl]ethylenediamine (Aldrich) according to the methods described in the literature [35,36]. In a typical synthesis, 1.5 g of MCM-41 or MCM-48 was dehydrated under vacuum at 473 K for 2 h in a Schlenk tube and then 50 ml of anhydrous toluene containing 2 ml of aminoalkylsilanes such as 3-aminopropytrimethoxysilane (1N-functional reagent, Aldrich) and *N*-[(3-trimethoxysilyl)-propyl]ethylenediamine (2N-functional reagent, Aldrich) was added. The mixture was filtered after being stirred for 24 h at 383 K under Ar. The solid was washed repeatedly with dry toluene and dried at 323 K under vacuum for 12 h. The functionalized silicas were designated as 1N- and 2N-support, respectively.

Supported Cu catalysts were prepared by mixing the supports with an ethanol solution of a calculated amount of $CuCl_2{\cdot}2H_2O$ (purity 99.5%) under Ar for 6 h, followed by evaporation to remove the solvent under vacuum and by vacuum drying at 383 K for 12 h. The loadings of $CuCl_2$ were varied in the range of 5–20 wt% based on Cu/support. The samples were designated as $CuCl_2$/1N-MCM-41, $CuCl_2$/2N-MCM-41, $CuCl_2$/1N-MCM-48, $CuCl_2$/2N-MCM-48, etc., respectively.

2.2. Catalytic oxy-carbonylation of methanol

The catalytic test was performed with a fixed-bed flow microreactor in the temperature range 373–423 K under the reaction conditions of GHSV = 1200 $ml\,h^{-1}\,g_{cat}^{-1}$ and $CO/CH_3OH/O_2/N_2 = 72/16/4/8$ (mol%) at 1.0 MPa. The mixture was regulated by mass-flow controllers. Methanol was introduced to the flow reactor by bubbling $CO/N_2/O_2$

mix gas through a stainless-steel saturator filled with methanol at a controlled temperature in order to obtain the molar ratio required. The outlet stream line from the reactor to a gas chromatograph was heated at about 423 K in order to avoid the condensation of reaction products. The products were analyzed by an on-line gas chromatograph using Porapak N (3 m) and AC (3 m) columns.

2.3. Catalyst characterization

The properties of the porous structures were determined from N_2-sorption measurements at 77 K using a Micromeritics ASAP 2010M+C system. The sample was outgassed under vacuum at 403 K for 3 h before the adsorption of nitrogen. The BJH method, based on the Kelvin equation, was applied to evaluate mesopore-size distribution by adsorption branch. The total pore volume for all samples was standardized versus the weight of pure mesoporous silicas by subtracting the organic amino group [36] and $CuCl_2$ loading weight. The microporous volume was evaluated by the t-plot method [37]. TG-DSC measurements were carried out on a Netzsch STA 449C thermal analyzer with a dynamic temperature program of 298–1400 K with a heating rate 10 K/min. The powder X-ray diffraction (XRD) patterns were measured on a Rigaku Rotaflex D/Max-C diffractometer. The analysis was carried out in a continuous $\theta/2\theta$ scan reflection mode using Cu-Kα radiation ($\lambda = 0.15418$). The anode was operated at 40 kV and 30 mA. The 2θ angles were scanned from 1.5 to 10° at a rate of 1°/min with slit parameters of DS = 0.5, SS = 0.5, and RS = 0.15. The 2θ angles were scanned from 10 to 70° at a rate of 2°/min with slit parameters of DS = 1, SS = 1, and RS = 0.15. The high-resolution TEM (HRTEM) images were obtained on a Philips TECNAI F-30 FEG instrument using accelerating voltage of 300 kV. The sample was dispersed with dry ethanol. The CHN elemental analyses were performed on a Perkin-Elmer series II CHNS/O analyzer 2400. Combustion temperature was set at 1248 K. The results of CHN elemental analyses were reported elsewhere [36].

The X-ray photoelectron spectroscopy (XPS) was measured with a PHI Quantum 2000 Scanning ESCA Microprobe equipment (Physical Electronics) using monochromatic Al-Kα radiation ($h\nu = 1846.6$ eV, 25 W). The background pressure in the analysis chamber was lower than 1×10^{-7} Pa. The X-ray beam diameter was 100 μm, and the pass energy was 29.5 eV for each analysis. The binding energy was calibrated using a C 1s photoelectron peak at 284.6 eV as a reference. The peak deconvolution and fitting were performed with a Gaussian–Lorentzian lineshape, fixing both spin–orbit splitting and the relative intensity of spin–orbit components.

The in situ Fourier transform infrared (in situ FT IR) measurements were carried out on a Perkin-Elmer Spectrum 2000 instrument with a MCT detector with a resolution of 4 cm^{-1}. The infrared spectra were recorded at beam temperature. Catalysts were pressed into self-supporting thin disks, which were placed in a quartz IR cell with CaF_2 windows, combined in a vacuum system. The samples were pretreated in the IR cell with temperature programs up to 423 K and at 423 K for 3 h under a dynamic vacuum (10^{-3} Pa). The sample was then cooled to 403 K. Dry CO of about 0.6 kPa was admitted to the system at 403 K. Subtraction of spectra from those before probe molecule adsorption shows bands due to adsorbed species.

3. Results

3.1. Methanol oxy-carbonylation on supported $CuCl_2$ catalysts

Previously, we have reported that a significant enhancement in the DMC production was obtained with $CuCl_2$ supported on 1N- or 2N-mesoporous silicas (MCM-41 and MCM-48) as catalysts in comparison to that with $CuCl_2$ supported on non-amino-functionalized silicas such as MCM-41, MCM-48, SiO_2, or 1N-SiO_2 and 2N-SiO_2 [33]. Additional experimental results showed that the lower catalytic performances for DMC production were obtained over the catalysts with $Cu(NO_3)_2$, $Cu(OAc)_2$, and $CuSO_4$ as copper precursors. Table 1 presents the atomic ratio of N/Cu versus the DMC yields with respect to the different Cu loadings in the catalysts of $CuCl_2$/1N-MCM-41 and $CuCl_2$/2N-MCM-41 at 403 K. The DMC yield increased with increasing Cu loadings and reached maximum values of 4.1 and 3.8 $g\,g_{Cu}^{-1}\,h^{-1}$, respectively, at 10 wt% $CuCl_2$. Above this loading the yield for DMC production tends to decline quickly. The highest DMC yield with $CuCl_2$ loadings at about 10 wt% was corresponding to the atomic ratio of N/Cu at about 1.5–2.4, depending on the type of amino-functional reagents employed.

Fig. 1 shows the methanol conversion, the selectivity of methanol and CO to DMC, and the DMC yield as a function of reaction temperature over the catalyst of 10 wt% $CuCl_2$/1N-MCM-41. The methanol conversion increased while the methanol selectivity to DMC decreased with the temperatures ranging from 373 to 433 K, whereas the best CO selectivity to DMC was obtained at about 393 K. The DMC yield passed through a maximum of 4.1 $g\,g_{Cu}^{-1}\,h^{-1}$ at 403 K. Higher reaction temperatures caused decreases in the selectivities of CO and methanol to DMC and also the DMC yield.

Fig. 2 depicts the DMC yield as a function of time on stream at 403 K with the catalysts of $CuCl_2$/1N-MCM-41, $CuCl_2$/2N-MCM-41, and $CuCl_2$/MCM-41 at 10 wt% of Cu-loading weight, respectively. The initial DMC production with $CuCl_2$/MCM-41 was higher than the amino-containing catalysts but it began to decrease after 2 h and became nearly zero after 4 h. However, quite different catalytic features were obtained with the catalysts of $CuCl_2$/2N-MCM-41 and $CuCl_2$/MCM-41, where the

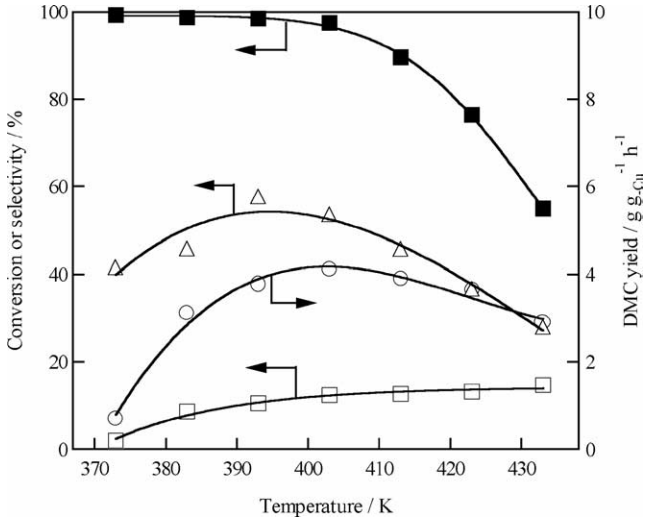

Fig. 1. Variations of conversion, selectivity, and DMC yield with temperature in the oxy-carbonylation of methanol to DMC on the 10 wt% $CuCl_2$/1N-MCM-41 catalyst. The reaction conditions are the same as in Table 1. ■, Methanol/DMC selectivity; △, CO/DMC selectivity; ◯, DMC yield; □, methanol conversion.

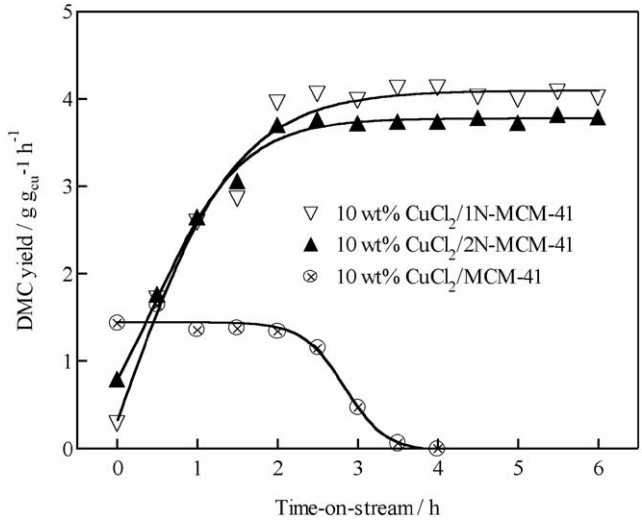

Fig. 2. DMC yield as a function of time on stream with the catalysts of $CuCl_2$/1N-MCM41, $CuCl_2$/2N-MCM-41, and $CuCl_2$/MCM-41 at 10 wt% of Cu-loading. Other reaction conditions are the same as in Table 1.

DMC production increased gradually during the initial 2 h and then remained essentially stable around 4.1 and 3.8 g g_{Cu}^{-1} h^{-1} for 6 h. Longer catalytic tests have been examined with the catalysts of 10 wt% $CuCl_2$/1N-MCM-41 and 10 wt% $CuCl_2$/2N-MCM-41 at 403 K. The catalytic activities began to decrease after about 12–14 h of running, but the DMC yields of 2.8 and 1.7 g g_{Cu}^{-1} h^{-1} were still obtained with the two catalysts after 30 h of reaction, respectively. The results revealed that the $CuCl_2$-supported 1N-functionalized mesoporous silicas exhibited a better stability in the catalytic oxy-carbonylation of methanol to produce the DMC.

3.2. Characterization by XRD, BET, and TG-DTA

Infrared spectra (not shown) of MCM-41 and MCM-48 showed that the bands at 2928, 2858, 1669, 1604, 1458, and 1352 cm^{-1} appeared at the expense of the band at 3742 cm^{-1} after amino-silylation, which were assigned to C–H asymmetric stretching, C–H symmetric stretching, NH_2 scissor, CH_2 scissor, and CH_3 bending vibrations, respectively. The band positions were similar to those reported in the literature [36,38]. The presence of the CH_3 bending mode suggested a small amount of remaining OCH_3.

Figs. 3 and 4 compare the X-ray diffraction patterns of MCM-41 and MCM-48 before and after functionalization with aminosilanes, and after immobilization of $CuCl_2$, respectively. The interplanar distance (d_{100}) and the hexagonal

Table 1
N/Cu ratio[a] and DMC yield for the catalysts of $CuCl_2$/1N-MCM-41 and $CuCl_2$/2N-MCM-41 with different $CuCl_2$ loadings[a]

Cu loading (wt%)	N/Cu[b] (mol mol^{-1})	SSA[c] (m^2 g^{-1})	$V_{p\,tot}$[d] (cm^3 g^{-1})	d_{BJH}[e] (nm)	DMC yield (g g_{Cu}^{-1} h^{-1})
$CuCl_2$/1N-MCM-41					
0	–	755	0.61	2.7	0
5	2.8	707	0.55	2.3	2.6
10	1.5	597	0.51	2.3	4.1
15	1.0	310	0.32	2.4	2.4
20	0.7	303	0.38	2.3	2.9
$CuCl_2$/2N-MCM-41					
0	–	702	0.59	2.5	0
5	4.7	460	0.41	2.3	0.7
10	2.4	448	0.44	2.2	3.8
15	1.6	254	0.30	2.3	2.8
20	1.2	130	0.14	2.2	2.3

[a] Reaction condition: reaction temperature = 403 K; total pressure = 1.0 MPa; catalyst weight = 1.0 g; Cu loading weight = 10 wt%; $CO/CH_3OH/O_2/N_2$ = 72/16/4/8; GHSV=1200 h^{-1}. Data obtained after reaction for 2 h.
[b] Calculated from the CHN elemental analysis data and the weighted $CuCl_2$ amount.
[c] BET specific surface area.
[d] Total pore volume.
[e] Mean pore diameter determined by the BJH method.

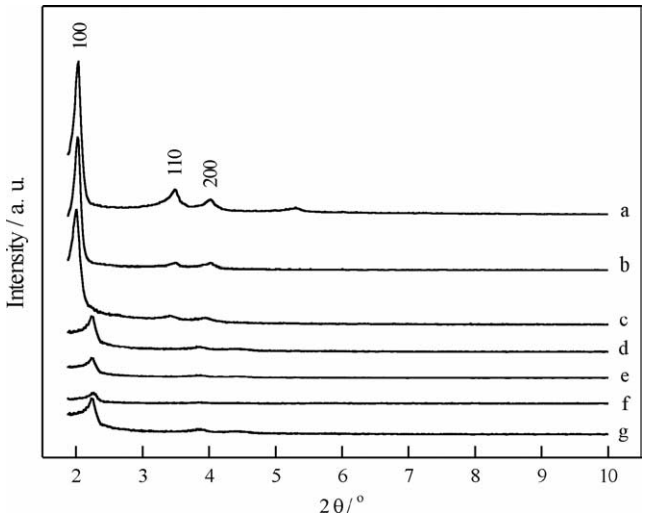

Fig. 3. XRD patterns for supports and as-prepared catalysts. (a) MCM-41; (b) 1N-MCM-41; (c) 2N-MCM-41; (d) 10 wt% $CuCl_2$/MCM-41; (e) 10 wt% $CuCl_2$/1N-MCM-41; (f) 10 wt% $CuCl_2$/2N-MCM-41; (g) 10 wt% $CuCl_2$/2N-MCM-41 after the reaction for 6 h.

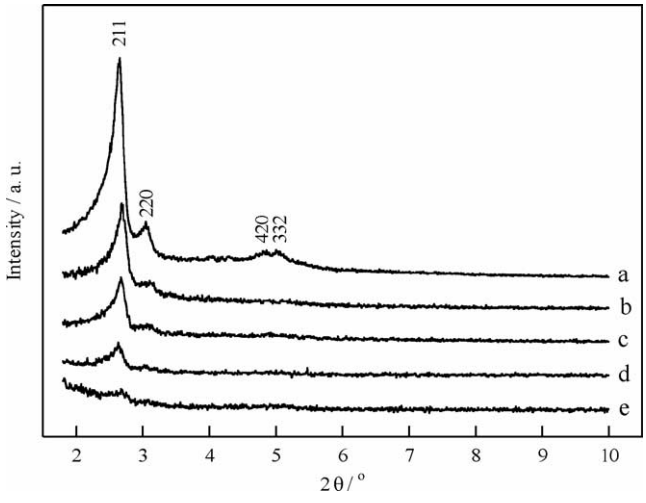

Fig. 4. XRD patterns for supports and as-prepared catalysts. (a) MCM-48, (b) 1N-MCM-48; (c) 2N-MCM-48; (d) 10 wt% $CuCl_2$/1N-MCM-48; (e) 10 wt% $CuCl_2$/2N-MCM-48.

unit cell parameter ($a_0 = 2d_{100}/\sqrt{3}$) of the MCM-41 and relevant catalysts are reported in Table 2. In the patterns of MCM-41, a dominant (100) peak with small (110) and (200) reflections was attributed to the 2D-hexagonal structure ($p6mm$). Aminosilane grafting to MCM-41 or MCM-48 and further $CuCl_2$ immobilizing on amino-functionalized ones caused a considerable decrease in the XRD intensity. The reflections due to higher indices almost disappeared and also the (100) reflection peak became very weak for the catalyst with 10 wt% of $CuCl_2$. The changes in Figs. 3 and 4 might be due to a partial loss of the space correlation of the pores. This kind of resultant disorder in silica mesostructures was commonly observed in studies of silylation and immobilization of mesoporous silicas [35]. Moreover, we found that the XRD intensities for the peaks due to hexagonal/cubic indices were slightly increased with no shifts in peak positions after the catalytic run for 10 h, suggesting there was no destruction of the mesoporous structures but redispersion of the catalytic sites during the reaction.

Large-angle XRD patterns for the $CuCl_2$/1N- and 2N-MCM-41 catalysts are shown in Fig. 5. The typical XRD diffraction lines for $CuCl_2$ appeared in the case of 10 wt% $CuCl_2$ supported on MCM-41 (Fig. 5k), while the diffraction lines essentially due to the crystalline $CuCl_2$ at the catalyst $CuCl_2$/2N-MCM-41 were only observed when the $CuCl_2$ loadings were higher than 10 wt%, although the weak patterns due to the crystalline $CuCl_2$ at the catalyst $CuCl_2$/1N-MCM-41 were visible at $CuCl_2$ loading of 10 wt%. Analogous results were obtained in the case of $CuCl_2$/1N-MCM-48 and $CuCl_2$/2N-MCM-48.

The curves of N_2 adsorption isotherms (not shown) of the pure-silica MCM-41 displayed a type IV isotherm with H1 hysteresis and a sharp increase in volume adsorbed at $P/P_0 = 0.4$, characteristic of highly ordered mesoporous materials. For samples of the functionalized supports and the corresponding catalysts, as a common feature, they exhibited type IV isotherms and a sharp increase in volume adsorbed at $P/P_0 = 0.2$ with lower specific area and smaller pore volume. The BJH pore-size distributions calculated from the adsorption branches were also smaller than that of MCM-41 (Tables 1 and 2). A careful t analysis, adopting as a refer-

Table 2
The textural property, pore structure, and DMC yield of the MCM-41 and relevant catalysts

Sample	SSA[a] ($m^2\,g^{-1}$)	$V_{p\,tot}$[b] ($cm^3\,g^{-1}$)	V_μ[c] ($cm^3\,g^{-1}$)	d_{100}[d] (nm)	α_0[e] (nm)	d_{BJH}[f] (nm)	DMC yield ($g\,g_{Cu}^{-1}\,h^{-1}$)
MCM-41	1051	0.99	0	4.33	5.00	3.5	0.0
1N-MCM-41	755	0.61	0	4.37	5.05	2.7	0.0
2N-MCM-41	702	0.59	0	4.40	5.08	2.5	0.0
10 wt% $CuCl_2$/MCM-41	801	0.82	0	3.96	4.57	2.7	1.4
10 wt% $CuCl_2$/1N-MCM-41	597	0.51	0	3.94	4.55	2.3	4.1
10 wt% $CuCl_2$/2N-MCM-41	448	0.44	0	3.93	4.54	2.2	3.8

[a] BET specific surface area.
[b] Total pore volume.
[c] Micropore volume.
[d] XRD (100) interplanar spacing.
[e] Hexagonal unit cell parameter, $a_0 = 2d_{100}/\sqrt{3}$.
[f] Mean pore diameter determined by the BJH method.

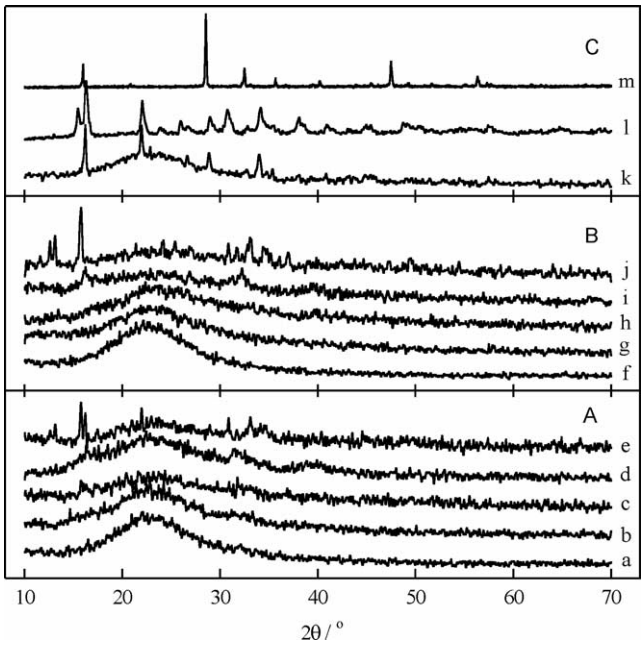

Fig. 5. Large-angle XRD patterns for as-prepared catalysts and the samples for reference. (A) $CuCl_2$/1N-MCM-41, Cu loading (wt%) at (a) 0; (b) 5; (c) 10; (d) 15; (e) 20. (B) $CuCl_2$/2N-MCM-41, Cu loading (wt%) at (f) 0; (g) 5; (h) 10; (i) 15; (j) 20. (C) (k) 10 wt% $CuCl_2$/MCM-41; (l) $CuCl_2$; (m) CuCl.

ence a nonporous silica isotherm reported in the literature [37,39], led to excluding the presence of micropores in all samples listed in Table 2. The results implied that the considerable amounts of organic groups and Cu species were essentially located in the inner channel of mesoporous silicas.

Fig. 6 shows the DSC profiles for the MCM-41, 1N-MCM-41, and 10 wt% $CuCl_2$/1N-MCM-41, respectively. The upward and downward peaks represented the endothermic and the exothermic processes during the heating, respectively. The small endothermic peaks at about 343–373 K were due to the vaporization of adsorbed water molecules at the samples. As for the 1N-MCM-41, a strong exothermic peak appeared at about 588 K (Fig. 6b), which was attributed to the decomposition of amino groups at the MCM-41 surfaces. In the case of the $CuCl_2$/1N-MCM-41, the exothermic process occurred at 433 K, peaking at 523 K (Fig. 6c), indicating that the decomposition temperature for the $CuCl_2$/1N-MCM-41 was lower than that of the 1N-MCM-41.

3.3. Characterization by HRTEM

The as-prepared samples of 1N-MCM-41, 2N-MCM-41, 10 wt% $CuCl_2$/1N-MCM-41, and 20 wt% $CuCl_2$/1N-MCM-41 were then imaged by high-resolution transmission electron microscopy shown in Fig. 7a–7d. No dramatic differences could be observed among the images of the intact MCM-41 (not shown), the amino-functionalized ones, and the catalyst with 10 wt% of $CuCl_2$ loading as revealed in Fig. 7a–7c. In contrast, the electron micrograph for 20 wt%

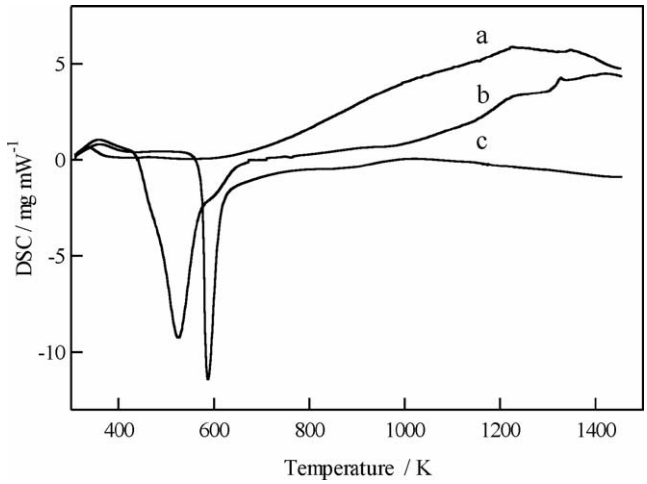

Fig. 6. The TG-DTA profiles for (a) MCM-41; (b) 1N-MCM-41; and (c) 10 wt% $CuCl_2$/1N-MCM-41 under air.

$CuCl_2$/1N-MCM-41 in Fig. 8d shows a more or less amorphous area and some dark spots which were covered at regular hexagonal arrays of support, reflecting that the dispersion of a considerable amount of $CuCl_2$ at the catalyst surfaces would not be uniform and homogeneous, probably due to the crystalline $CuCl_2$ as evidenced by XRD. The results revealed that the whole characteristic features of the regular hexagonal array were essentially retained in the functionalized MCM-41 and the catalyst thus prepared, and also a high dispersion of the Cu species was obtained at the surfaces of amino-functional mesoporous silicas in the case of $CuCl_2$ loading weights less than 10 wt% under the present preparation conditions.

3.4. Characterization by XPS and FTIR

To examine the structural information and the redox properties for $CuCl_2$/MCM-41 and $CuCl_2$/1N-MCM-41 catalysts, measurements of ex situ XPS and in situ FTIR have been carried out respectively. The Cu 2p XPS spectra for the as-prepared $CuCl_2$/1N-MCM-41 with different Cu loadings are showed in Fig. 8. For comparison the Cu 2p XPS for the as-prepared 10 wt% $CuCl_2$/MCM-41 has also been incorporated. There were two intense peaks at 934.9/954.7 eV for $CuCl_2$/MCM-41 (Fig. 8a) assignable to Cu^{2+} $2p_{3/2}$ and $2p_{1/2}$, along with corresponding Cu^{2+} satellite peaks at 942.3–944.8 eV. The Cu^+ species were often formed during the $CuCl_2$/MCM-41 preparation. The Cu 2p XPS spectra for the catalyst $CuCl_2$/1N-MCM-41 with Cu loading of 5 wt% exhibited two peaks at 932.4 and 952.2 eV, which are attributable to Cu $2p_{3/2}$ and Cu $2p_{1/2}$ levels of Cu^+ species. For the catalyst with a Cu loading of 10 wt%, however, the weak XPS Cu 2p peaks at 934.9/954.7 eV for Cu^{2+} species appeared, in addition to the strong peaks for Cu^+. In the case of $CuCl_2$/2N-MCM-41, the Cu $2p_{3/2}$ and Cu $2p_{1/2}$ levels of Cu^{2+} species were only observed if the Cu loadings above 10 wt% (not shown). These XPS observations are in good agreement with the XRD results in Fig. 5.

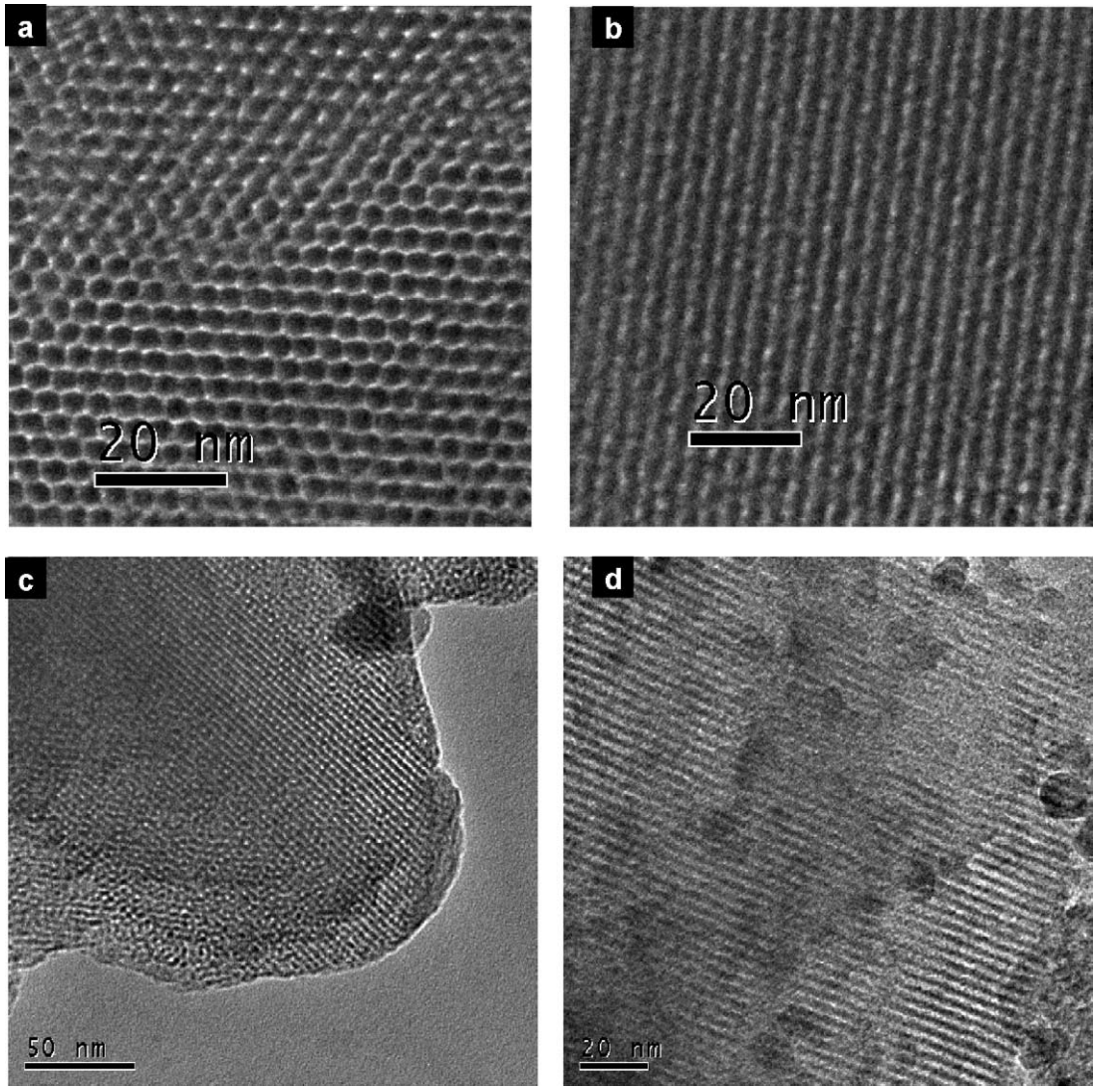

Fig. 7. HRTEM micrographs for as-prepared samples of (a) 1N-MCM-41 in the direction of pore axis; (b) 2N-MCM-41 in the direction perpendicular to the pore axis; (c) 10 wt% $CuCl_2$/2N-MCM-41 in the direction perpendicular to the pore axis; and (d) 20 wt% $CuCl_2$/1N-MCM-41 in the direction perpendicular to the pore axis.

Fig. 9 shows Cu 2p XPS spectra for the catalysts $CuCl_2$/1N-MCM-41 and $CuCl_2$/2N-MCM-41 with 10 wt% loading before and after reaction at 403 K for 10 h. The catalysts before and after oxy-carbonylation of methanol at 403 K exhibited no significant difference in the Cu 2p XPS peak positions, although there was a slight broadness in the peak intensities. The results demonstrated that Cu species were strongly interacted with supports.

The structural information and the electronic properties were further examined by in situ FTIR spectroscopy for CO adsorbed on the catalysts of $CuCl_2$/MCM-41, $CuCl_2$/1N-MCM-41, and $CuCl_2$/2N-MCM-41 with 10 wt% $CuCl_2$ loading weight at 403 K, respectively. The results are illustrated in Fig. 10. When about 0.6 kPa of CO was admitted into $CuCl_2$/MCM-41 in an in situ IR cell at 403 K, bands at 2209, 2190, 2156, and 2134 cm^{-1} were observed as shown in Fig. 10a. Evacuation of the system at 403 K caused a quick decrease in intensity. Under identical conditions, the peaks of adsorbed CO on $CuCl_2$/1N-MCM-41 were observed at 2170, 2131, and 2117 cm^{-1} and on $CuCl_2$/2N-MCM-41 at 2170, 2131, and 2110 cm^{-1}, respectively. Recently, Knözinger et al. obtained similar results of FTIR spectroscopy of adsorbed CO on the oxidized and reduced samples of Cu/MCM-41 and Cu/MCM-48 [40]. In the case of $CuCl_2$/MCM-41, the band at 2156 was attributed to OH–CO species and the ones at 2209–2190 cm^{-1} are characterized to the carbonyls of Cu(II) cations. The 2134 cm^{-1} band was attributed to physically adsorbed CO. In the cases of $CuCl_2$/1N-MCM-41 and $CuCl_2$/2N-MCM-41, the 2170 cm^{-1} band was due to OH–CO species, while the bands at 2110–2117 cm^{-1} were assignable to the reduced (electron-rich) Cu^+–CO species.

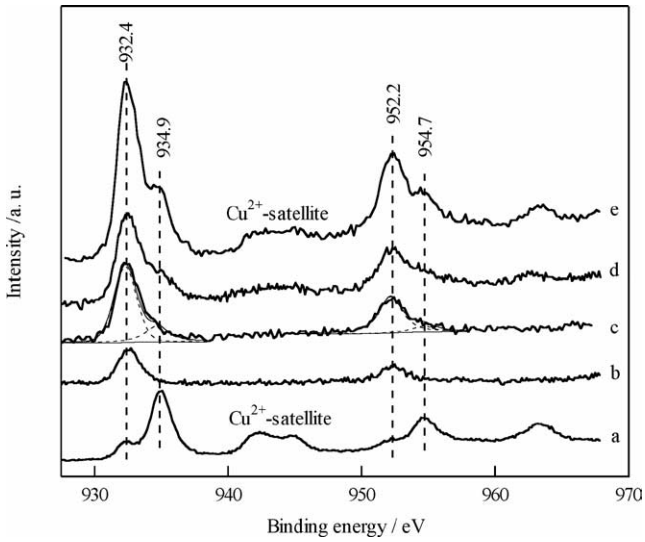

Fig. 8. Cu 2p XPS spectra for the $CuCl_2$/1N-MCM-41 catalysts; Cu loading (wt%) at (a) 0; (b) 5; (c) 10; (d) 15; (f) 20.

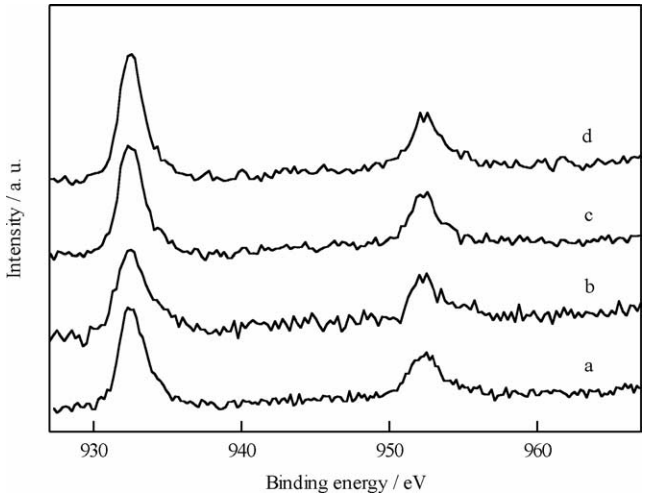

Fig. 9. Cu 2p XPS spectra for the catalysts before and after the reaction for 6 h, Cu loading = 10 wt%. (a) As-prepared $CuCl_2$/1N-MCM-41; (b) $CuCl_2$/1N-MCM-41 after the reaction; (c) as-prepared $CuCl_2$/2N-MCM-41; (d) $CuCl_2$/2N-MCM-41 after the reaction.

4. Discussion

4.1. Catalytic properties of supported $CuCl_2$ for the selective oxy-carbonylation of methanol to DMC

It was found that the $CuCl_2$ supported on amino-functionalized ordered mesoporous silicas MCM-41 and MCM-48 by a simple and versatile scheme of impregnation are excellent catalyst candidates for the vapor-phase oxy-carbonylation of methanol to DMC. The catalysts are air stable and reusable when the reaction temperatures were not higher than 433 K as evidenced by the results of durability tests in Fig. 2 and DSC characterization in Fig. 6. The highest reaction rates on $CuCl_2$/1N-MCM-41 and $CuCl_2$/2N-MCM-41 catalysts were achieved at a Cu loading of 10 wt%. We

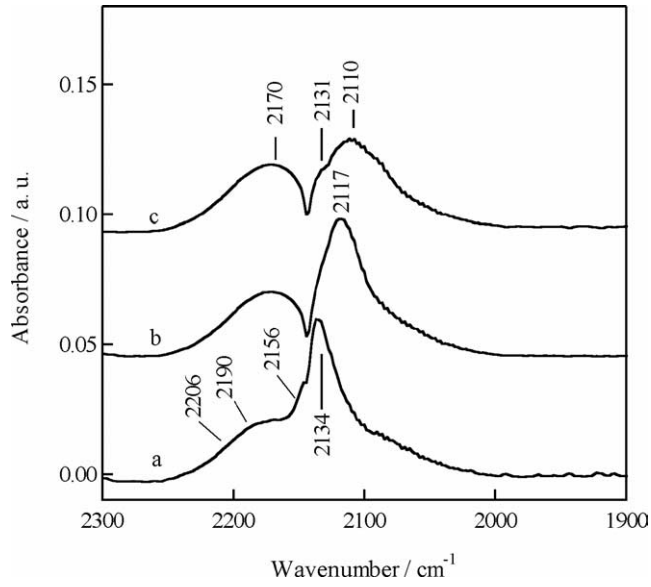

Fig. 10. In situ FT IR spectra for the CO adsorption on (a) 10 wt% $CuCl_2$/MCM-41; (b) 10 wt% $CuCl_2$/1N-MCM-41; (c) 10 wt% $CuCl_2$/2N-MCM-41.

have compared the catalytic results with $CuCl_2$ supported on amorphous SiO_2 with and without amino-functionalization and found that there was not much difference in the catalytic activity between the catalysts generated from amorphous SiO_2 and amino-functionalized ones. Also, the catalyst prepared from the amino-functionalized amorphous silica was much less efficient than that from the amino-functionalized MCM-41 or the amino-functionalized MCM-48 [33].

As expected, the N/Cu ratios (molar ratio) of $CuCl_2$/2N-MCM-41 were higher than those of $CuCl_2$/1N-MCM-41 in the $CuCl_2$ loadings ranging from 5 to 20 wt% as calculated by CHN elemental analysis data (Table 1). The number of nitrogen atoms in one molecule of 2N-reagent was twice that in the 1N-reagent, but the nitrogen contents in the amino-functionalized mesoporous silicas and the corresponding catalysts did not show such a ratio. This result probably suggested that there existed spatial hindrance during the grafting in the case of attaching *N*-[(3-trimethoxysilyl)propyl]ethylenediamine onto the mesoporous silicas. Moreover, the N/Cu ratios were larger than 1.0 when the $CuCl_2$ loading weight was below 10 wt% in the catalyst $CuCl_2$/1N-MCM-41 and even if the $CuCl_2$ loading weight was at 20 wt% in the case of $CuCl_2$/2N-MCM-41. The highest activity, however, was obtained with 10 wt% $CuCl_2$ loading, which corresponds to the N/Cu ratio of 1.5/1 and 2.4/1 in $CuCl_2$/1N-MCM-41 and $CuCl_2$/2N-MCM-41, respectively (Table 1).

The results in Table 1 also showed that the ordered mesoporous silicas with uniform pores in diameters of 2–3 nm were suited to accommodate the amino groups and $CuCl_2$ as reflected by the moderate decreases in the surface areas and pore volumes. The uniform pores and surface areas after the amino-functionalization and immobilization of $CuCl_2$ were possible to provide appropriate spaces for diffusion and reac-

tion of the reactant molecules. As for the 1N-(or 2N-)SiO_2, however, much lower specific surface areas than those in the intact one were obtained, probably due to the "block" of the amino reagents to the micropores which were known as the main contribution to the surface area of amorphous SiO_2 [33]. The catalysts thus prepared showed low catalytic activity in the DMC production.

4.2. Structure feature of supported $CuCl_2$ catalysts

The shifts in the XRD peaks for MCM-41 and MCM-48 (Figs. 3 and 4) after immobilization of $CuCl_2$ are true and common in studies of silylation and immobilization of mesoporous silicas [35], not due to a sample misalignment of XRD patterns (along the 2θ axis). One explanation may be due to the amino groups and $CuCl_2$ species in the pore channel after the immobilization, which enhanced the thickness of pore wall, but disturbed the regular periodic variation of the electron density, resulting in the apparent decrease of hexagonal symmetry. Considering the unit cell parameter (α_0) and mean pore size (d_{BJH}) reported in Table 2, it is possible to calculate the size of silicate walls (s) around the hexagonal arrangement of the cylindrical pores by the equation of $\alpha = d_{BJH} + s$. The sizes of the silicate walls were 1.5, 2.35, and 2.58 nm for MCM-41, 1N-MCM-41, and 2N-MCM-41, and 1.87, 2.25, and 2.34 nm for 10 wt% $CuCl_2$/MCM-41, 10 wt% $CuCl_2$/1N-MCM-41, and 10 wt% $CuCl_2$/2N-MCM-41, respectively. The increasing size of pore walls might be correlated to the decrease in the order, as observed in the XRD patterns (Fig. 3). The HRTEM micrographs (Fig. 7) confirmed that the whole characteristic features of the regular hexagonal array were essentially retained in the amino-functionalized MCM-41 and the catalysts with $CuCl_2$ loading lower than 20 wt%, although the reflections due to higher indices almost disappeared and also the (100) reflection peak became considerably weak.

In the samples with $CuCl_2$ loading lower than 10 wt% the electron-rich Cu species likely Cu^+ were essentially observed, while in those above 10 wt% loading the free Cu^{2+} species emerged, whether the support was 1N-MCM-41 or 2N-MCM-41, as evidenced by XRD, XPS, and HRTEM. The results, along with the observation of in situ FTIR spectroscopy in Fig. 10, indicated that the amino groups at the surfaces of ordered mesoporous silicas were electronically σ-donors to $CuCl_2$, probably forming the mono/bi/multidentate $(N)_n \rightarrow Cu^{2+}$ complex species ($n \geqslant 1$, depending on the Cu loadings). We deduced that the saturated coordination mode for Cu–N complexes was close to the form of $(N)_2 \rightarrow Cu$ (the molar ratio of N/Cu = 2). In such a case, the catalyst might be able to afford the highest activity. As for $CuCl_2$/2N-MCM-41, the nitrogen atoms that coordinated to the Cu species might principally be the amines at the end of amino groups due to the spatial hindrance.

Therefore, the interaction between $CuCl_2$ and amino-functional groups at the ordered mesoporous silicas forms a coordinative stabilization to Cu^{2+} sites with $(N)_2 \rightarrow Cu^{2+}$ complexation mode, affording electron-rich species likely Cu^+ in the XPS observation. The comparative studies of $CuCl_2$ supported on non-amino-functionalized silicas and amino-functionalized ones implied that the redox cycle of Cu^{2+}/Cu^+ species was accelerated by the coordination of amino groups with Cu^{2+} and mainly responsible for the enhancement in reaction rate in the oxy-carbonylation of methanol to DMC. In addition, the readily accessible active sites and the easy dischargeability for the reactants due to the regular mesopores of the supports might also be beneficial and necessary.

5. Conclusions

(1) Considerable enhancements in the reaction rate and catalytic stability with $CuCl_2$ supported onto amino-functionalized MCM-41 and MCM-48 in the DMC production via oxy-carbonylation of methanol have been obtained as compared to that with $CuCl_2$-supported nonfunctionalized mesoporous silicas under identical conditions. Better catalytic stability with $CuCl_2$/1N-MCM-41 over $CuCl_2$/2N-MCM-41 was obtained.

(2) The DMC yield increased with increasing $CuCl_2$ loading, and reached a maximum value at a loading weight of 10 wt% $CuCl_2$. The catalyst 10 wt% $CuCl_2$/1N-MCM-41 was structurally stable at temperatures lower than 433 K. The catalytic activity increased but the selectivity to DMC decreased with increasing reaction temperature, giving a maximum DMC yield at 403 K.

(3) The $CuCl_2$ species with loading amounts lower than 10 wt% were mainly located and dispersed in the mesopores of amino-functionalized mesoporous silicas. Such $CuCl_2$ species were mostly coordinated to the amino groups by forming mono/bi/multidentate moieties. The crystalline phases of $CuCl_2$ emerged when $CuCl_2$ loadings were higher than 10 wt%.

(4) The coordinative interaction between $CuCl_2$ and amino-functional groups at the ordered mesoporous silicas caused stabilization and dispersion of the Cu species. The redox capability of Cu species between Cu^{2+} and Cu^+ due to the nitrogen σ-donation was important for the enhancement in reaction rate in the oxy-carbonylation of methanol to DMC.

Acknowledgments

The authors gratefully acknowledge the financial support from the NSF of China (Grant 20021002) and MOE of China.

References

[1] J.S. Beck, J.C. Vartuli, W.J. Roth, M.E. Leonowicz, C.T. Kresge, K.D. Schmitt, C.T.W. Chu, D.H. Olson, E.W. Sheppard, S.B. McCullen, J.B. Higgins, J.L. Schlenkert, J. Am. Chem. Soc. 114 (1992) 10,834.

[2] D.E. De Vos, M. Dams, B.F. Sels, P.A. Jacobs, Chem. Rev. 102 (2002) 3615.
[3] O. Leal, D.L. Anderson, R.C. Bowman, F. Basolo, R.L. Burwell, J. Am. Chem. Soc. 97 (1975) 5125.
[4] I. Haller, J. Am. Chem. Soc. 100 (1978) 8050.
[5] P. Hernan, C. Pino, E.R. Huitzky, Chem. Mater. 4 (1992) 49.
[6] K. Miki, Y. Sato, Bull. Chem. Soc. Jpn. 66 (1993) 2385.
[7] B. Pugin, M. Müller, Stud. Surf. Sci. Catal. 78 (1993) 107.
[8] K.D. Behringer, J. Blümel, Chem. Commun. (1996) 653.
[9] A. Cauvel, G. Renard, D. Brunel, J. Org. Chem. 62 (1997) 749.
[10] D. Brunel, A. Cauvel, F. Fajula, F. DiRenzo, Stud. Surf. Sci. Catal. 97 (1995) 173.
[11] P. Sutra, D. Brunel, Chem. Commun. (1996) 2485.
[12] J.F. Diaz, K.J. Balkus Jr., F. Bedioui, V. Kurshev, L. Kevan, Chem. Mater. 9 (1997) 61.
[13] T. Kimura, S. Saeki, Y. Sagahara, K. Kuroda, Langmuir 15 (1998) 2794.
[14] G.E. James, C.H. James, D.J. Macquarrie, Synlett (1998) 625.
[15] J. Evans, A.B. Zaki, M.Y. El-Sheikh, S.A. El-Safty, J. Phys. Chem. B 104 (2000) 10,271.
[16] U. Romano, R. Tesel, M.M. Mauri, P. Rebora, Ind. Eng. Chem. Prod. Res. Dev. 19 (1980) 396.
[17] D. Delledonne, F. Rivetti, U. Romano, Appl. Catal. A 221 (2001) 241.
[18] G.L. Curuntt, D.C. Harley, Oxygen Complexes and Oxygen Activation by Transition Metals, Plenum, New York, 1988, pp. 215–232.
[19] S.T. King, J. Catal. 161 (1996) 530.
[20] S.T. King, Catal. Today 33 (1997) 173.
[21] Z. Li, K. Xie, R.C.T. Slade, Appl. Catal. A 205 (2001) 85.
[22] M.Y. Lee, D.C. Park, Stud. Surf. Sci. Catal. 66 (1991) 631.
[23] Y. Wang, X. Zhao, B. Yuan, B. Zhang, J. Cong, Appl. Catal. A 171 (1998) 255.
[24] K. Otsuka, T. Yagi, I. Yamanaka, Chem. Lett. (1999) 495.
[25] K. Tomishige, T. Sakaihori, S. Sakai, K. Fujimoto, Appl. Catal. A 181 (1999) 95.
[26] M.S. Han, B.G. Lee, I. Suh, H.S. Kim, B.S. Ahn, S.I. Hong, J. Mol. Catal. A: Chem. 170 (2001) 225.
[27] P. Yang, Y. Cao, J.-C. Hu, W.-L. Dai, K.-N. Fan, Appl. Catal. A 241 (2003) 363.
[28] Y. Sato, M. Kagotani, T. Yamamoto, Y. Souma, Appl. Catal. A 185 (1999) 219.
[29] Y. Sato, Y. Souma, Catal. Surveys Jpn. 4 (2000) 65.
[30] Y. Sato, M. Kagotani, Y. Souma, J. Mol. Catal. A 151 (2000) 79.
[31] V. Raab, M. Merz, J. Sundermeyer, J. Mol. Catal. A: Chem. 175 (2001) 51.
[32] Y. Cao, J.-C. Hu, W.-L. Dai, K.-N. Fan, Chem. Commun. (2003) 908.
[33] W. Cao, H.-B. Zhang, Y.-Z. Yuan, Catal. Lett. 91 (2003) 243.
[34] L.-Y. Chen, T. Horiuchi, T. Mori, K. Maeda, J. Phys. Chem. B 103 (1999) 1216.
[35] H. Yoshitake, T. Yokoi, T. Tatsumi, Chem. Mater. 14 (2002) 4603.
[36] Q.-R. Peng, Y. Yang, Y.-Z. Yuan, J. Mol. Catal. A: Chem. 219 (2004) 175.
[37] S. Storck, H. Bretinger, W.F. Maier, Appl. Catal. A 174 (1998) 137.
[38] H. Yoshitke, T. Yokoi, T. Tatsumi, Chem. Mater. 15 (2003) 1713.
[39] J.D. Carruthers, P.A. Cutting, R.E. Day, M.R. Harris, S.A. Mitchell, K.S.W. Sing, Chem. Ind. 50 (1968) 1772.
[40] K. Hadjivanov, T. Tsoncheva, C. Minchev, H. Knözinger, Appl. Catal. A 241 (2003) 331.